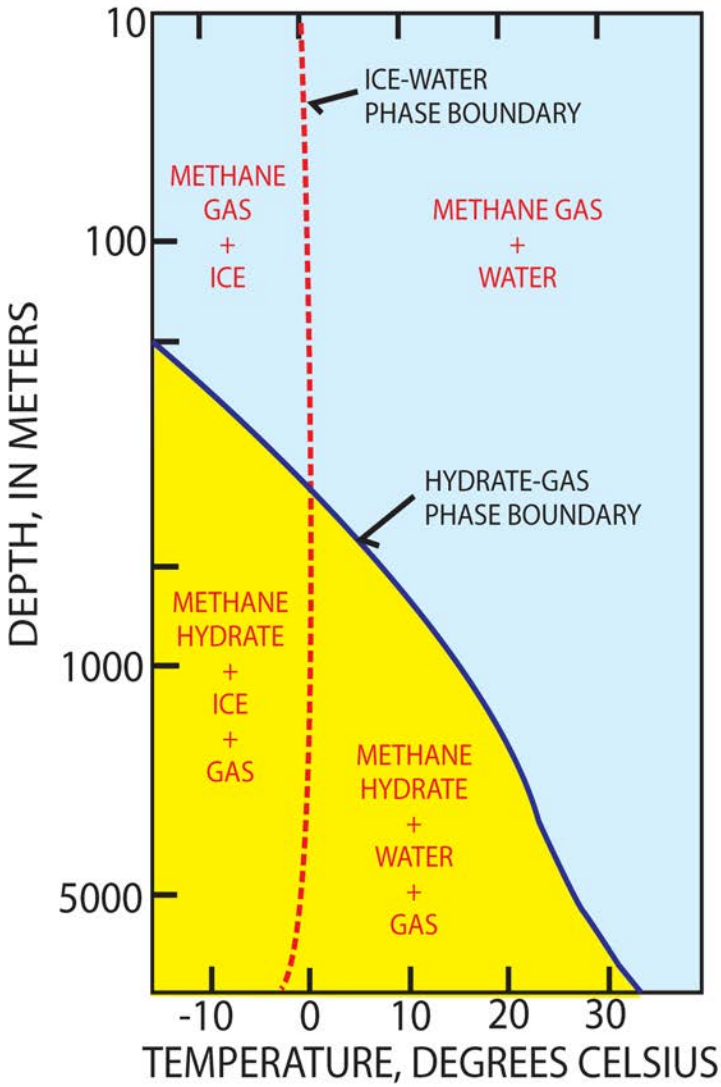

Figure 3.1. Pressure (depth) and temperature methane hydrate stability diagram (modified from Kvenvolden, 1988).

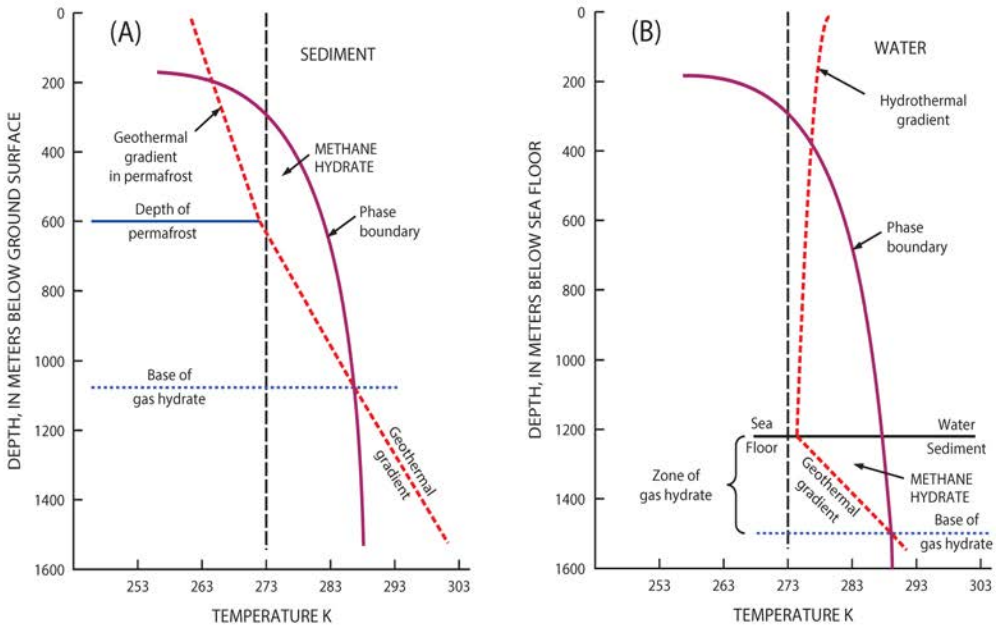

Figure 3.2. Arbitrary examples of different depth-temperature zones in which methane hydrates are stable: (A), a permafrost region; and (B), an outer continental margin marine setting (modified from Kvenvolden, 1988).

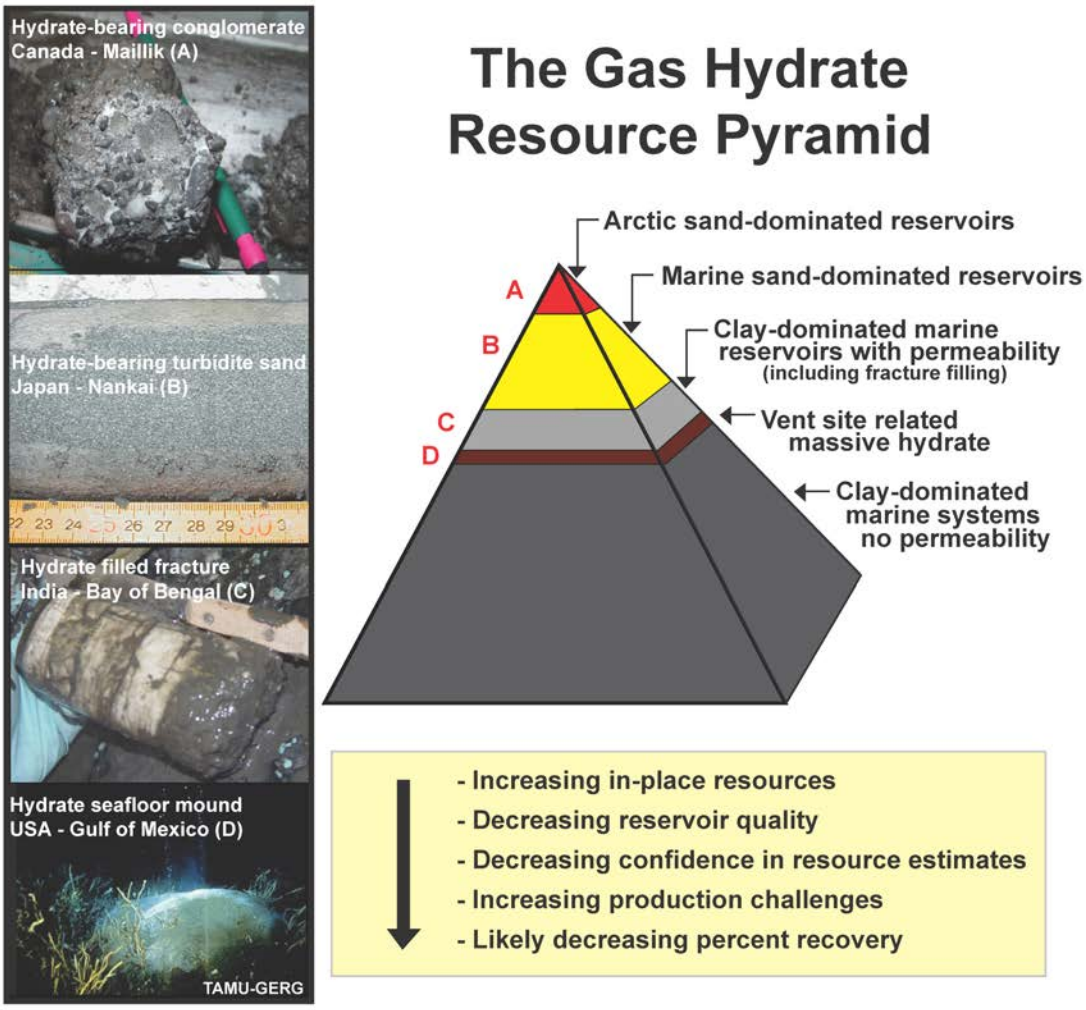

Figure 3.3. Methane hydrate resource pyramid depicting the types of expected methane hydrate occurrences. Also shown are images of various example methane hydrate occurrences (modified from Boswell and Collett, 2006).

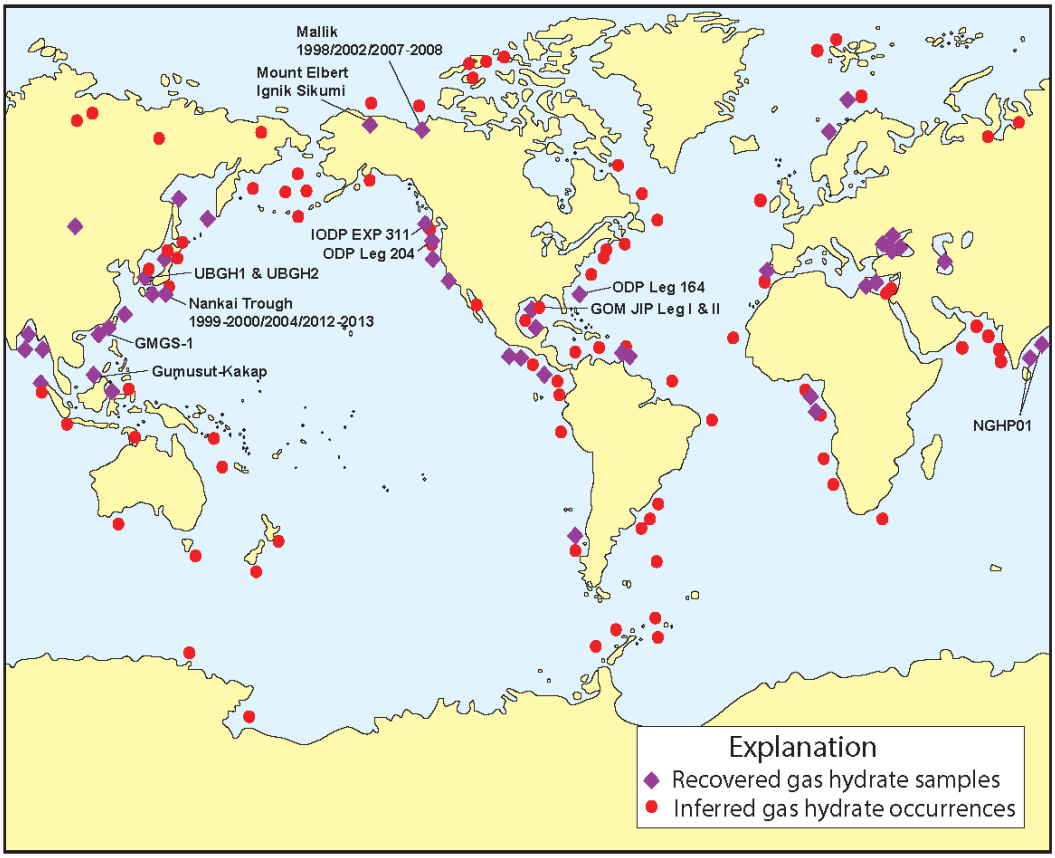

Figure 4.1. Location of sampled and inferred methane hydrate occurrences in oceanic sediment of outer continental margins and permafrost regions (modified from Kvenvolden, 1993). Most of the recovered methane hydrate samples have been obtained during deep coring projects or shallow seabed coring operations. Most of the inferred methane hydrate occurrences are sites at which bottom simulating reflectors (BSRs) have been observed on available seismic profiles. The methane hydrate research drilling projects and expeditions reviewed in this report have also been highlighted on this map.

Figure 4.2. Distribution of permafrost in the northern hemisphere (source of permafrost data: http://nsidc.org/data/ggd318.html). Shown are the areas of onshore continuous permafrost (dark blue) and of offshore possible relic permafrost (light blue) under which conditions may be favorable for the accumulation of methane hydrate (modified from Collett, 2002).

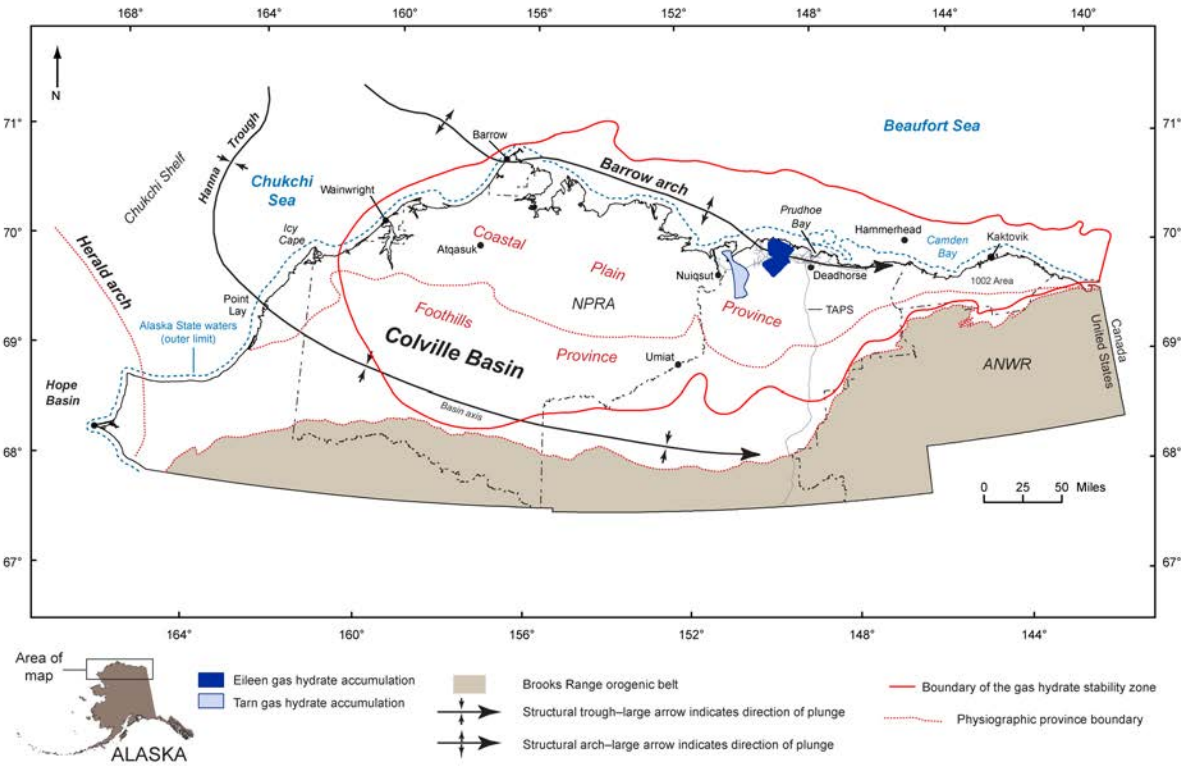

Figure 4.3. (A) Physiographic provinces and major tectonic features of the North Slope in Alaska (modified from Collett et al., 2008a). Also shown is the location of the Eileen and Tarn methane hydrate accumulations along with the limit of methane hydrate stability zone in northern Alaska (red outline). NPRA = National Petroleum Reserve in Alaska, ANWR = Arctic national Wildlife Refuge.

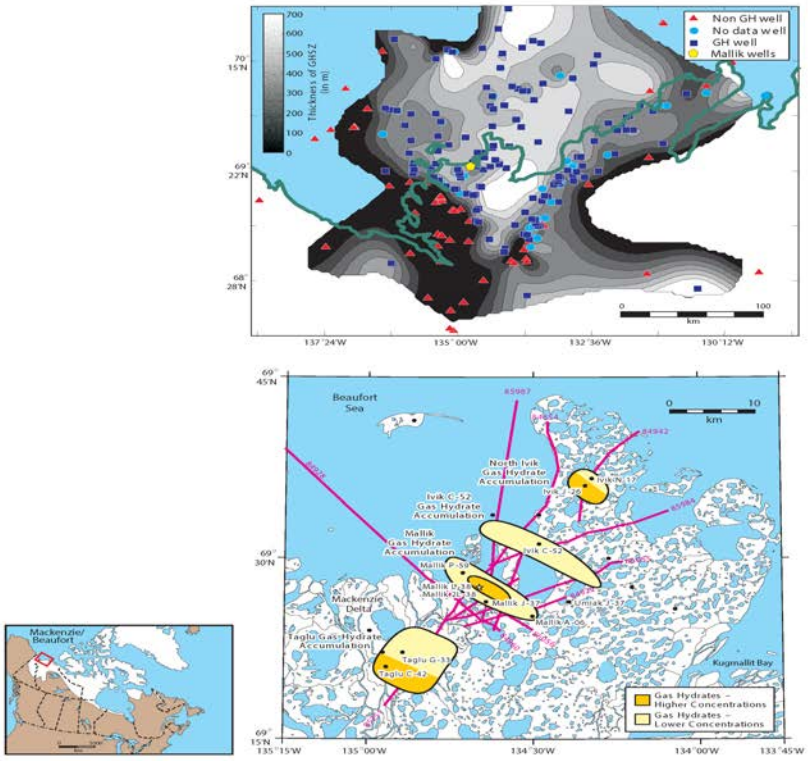

Figure 4.3. (B) Maps of the Mackenzie Delta region in Canada showing the location of industry exploratory wells with well-log-inferred hydrate occurrences (in upper map) and the limit of the methane hydrate stability zone in the Mackenzie Delta region (modified from Dallimore and Collett, 2005). Also shown (in lower map) are four seismic- and well-log-inferred methane hydrate accumulations in tan (modified from Dallimore et al., 1999).

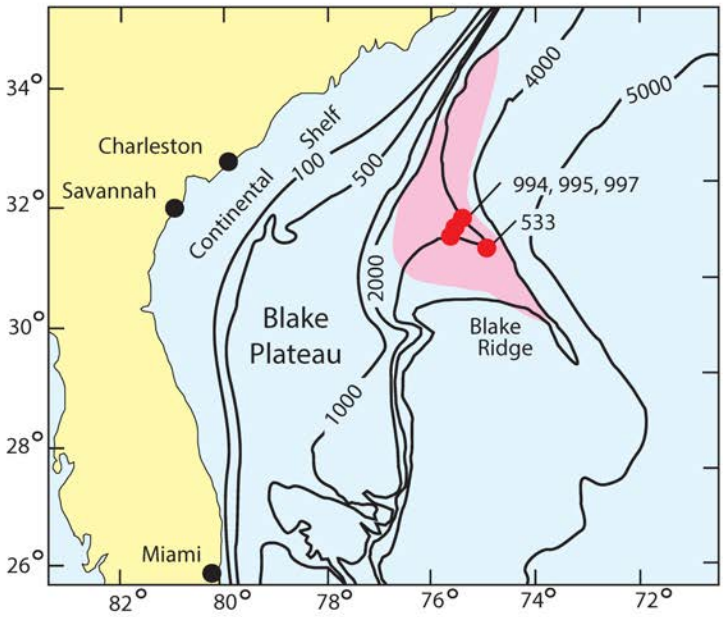

Figure 4.4. Map of the southeastern continental margin of North America. Location of DSDP Leg 76 Site 533 and ODP Leg 164 Sites 994, 995, and 997 are indicated. Also shown is the area (pink-shaded area) where methane hydrate has been mapped on the basis of bottom-simulating reflectors. Contours are depths of water in meters (modified from Shipboard Scientific Party, 1996).

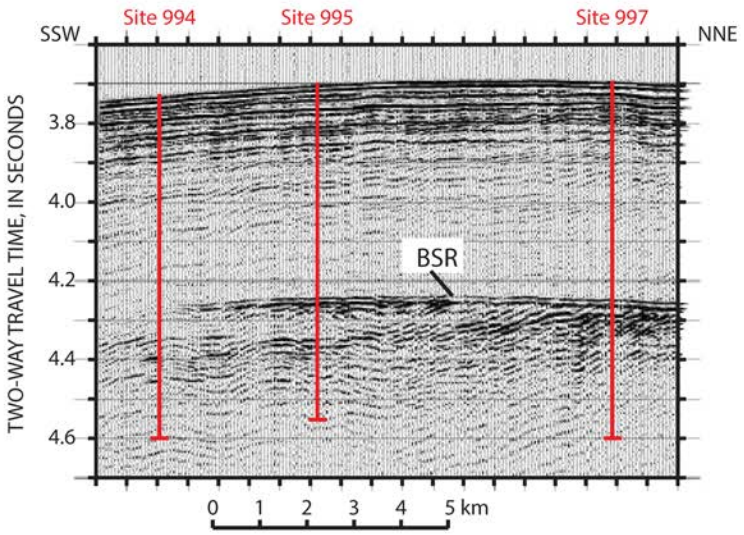

Figure 4.5. Seismic profile along which ODP Leg 164 Sites 994, 995, and 997 are located. Note that Site 994 is not associated with a distinct bottom-simulating reflector (BSR), although a strong BSR occurs at Sites 995 and 997 (modified from Shipboard Scientific Party, 1996).

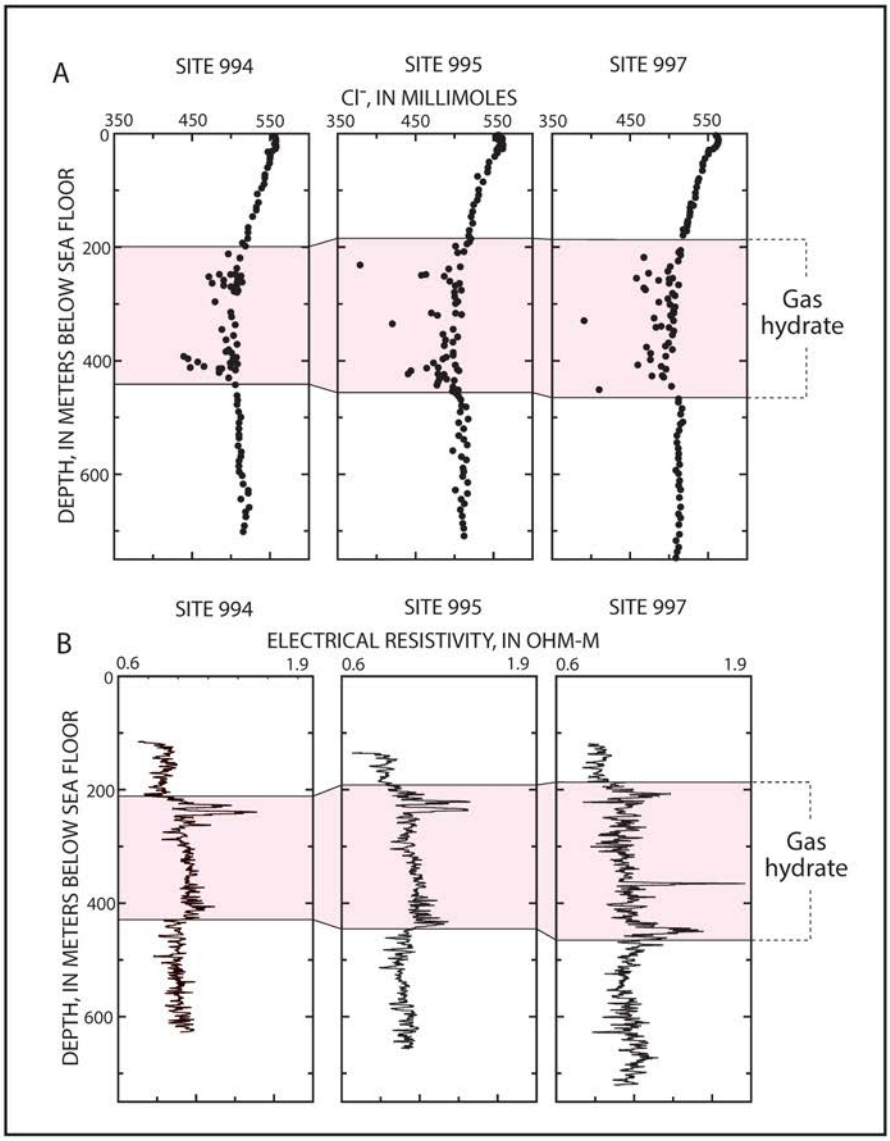

Figure 4.6. (A) Chloride concentration profiles for interstitial waters collected from cores at ODP Leg 164 Sites 994, 995, and 997. (B) Downhole electrical resistivity logs from ODP Leg 164 Sites 994, 995, and 997. Also shown is the chloride concentration and electrical resistivity inferred methane hydrate distribution (modified from Shipboard Scientific Party, 1996).

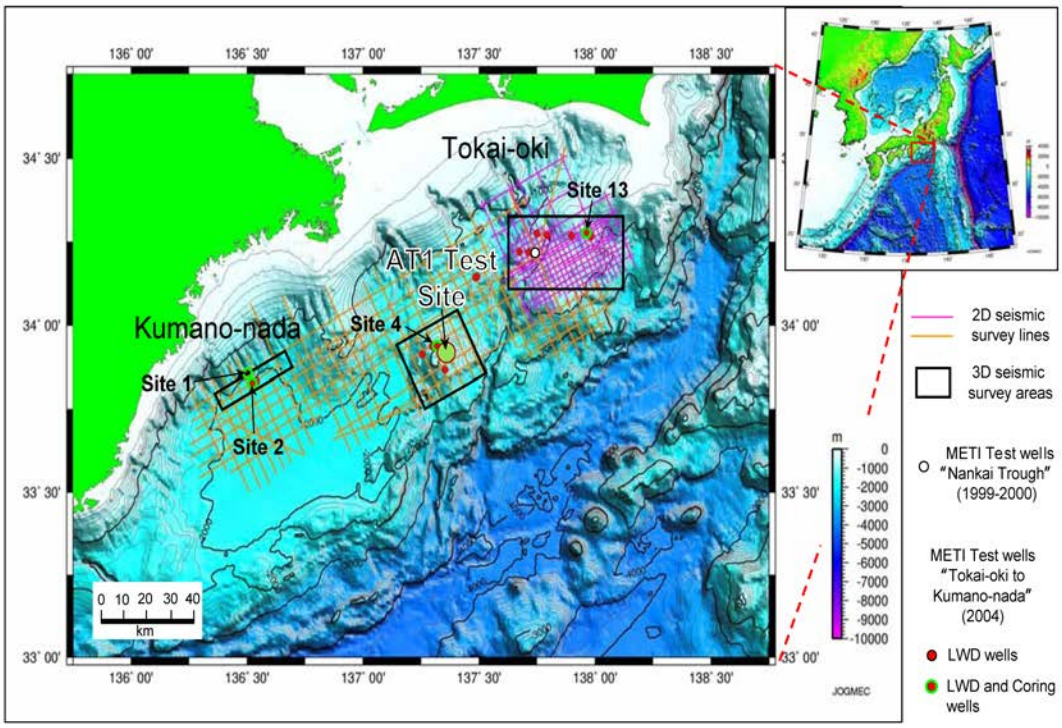

Figure 4.7. Map of Nankai Trough region along the southeast coast of Japan. Shown are the locations of the 1999/2000 METI wells and the 2004 Tokai-oki to Kumano-nada wells along with the location of the 2012/2013 AT1 Test Site. Also shown is the location of the 2D and 3D seismic data used to select the location of the sites drilled during both field efforts (modified from Fujii et al., 2009).

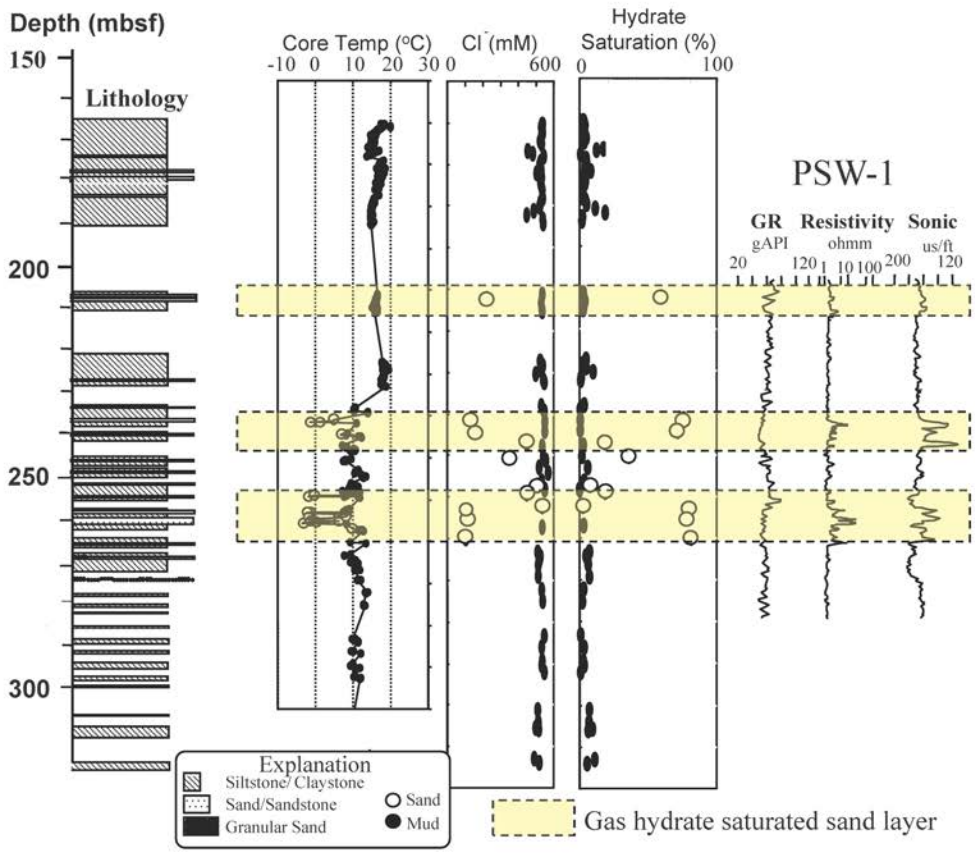

Figure 4.8. Downhole well log and core data display showing core derived lithology, recovered core temperatures, pore-water chloride (Cl^-) concentrations, and methane hydrate saturations derived from observed pore-water chloride freshening in the METI Nankai Trough well with additional well log data from the Post Survey 1 well (PSW-1) (modified from Uchida et al., 2009).

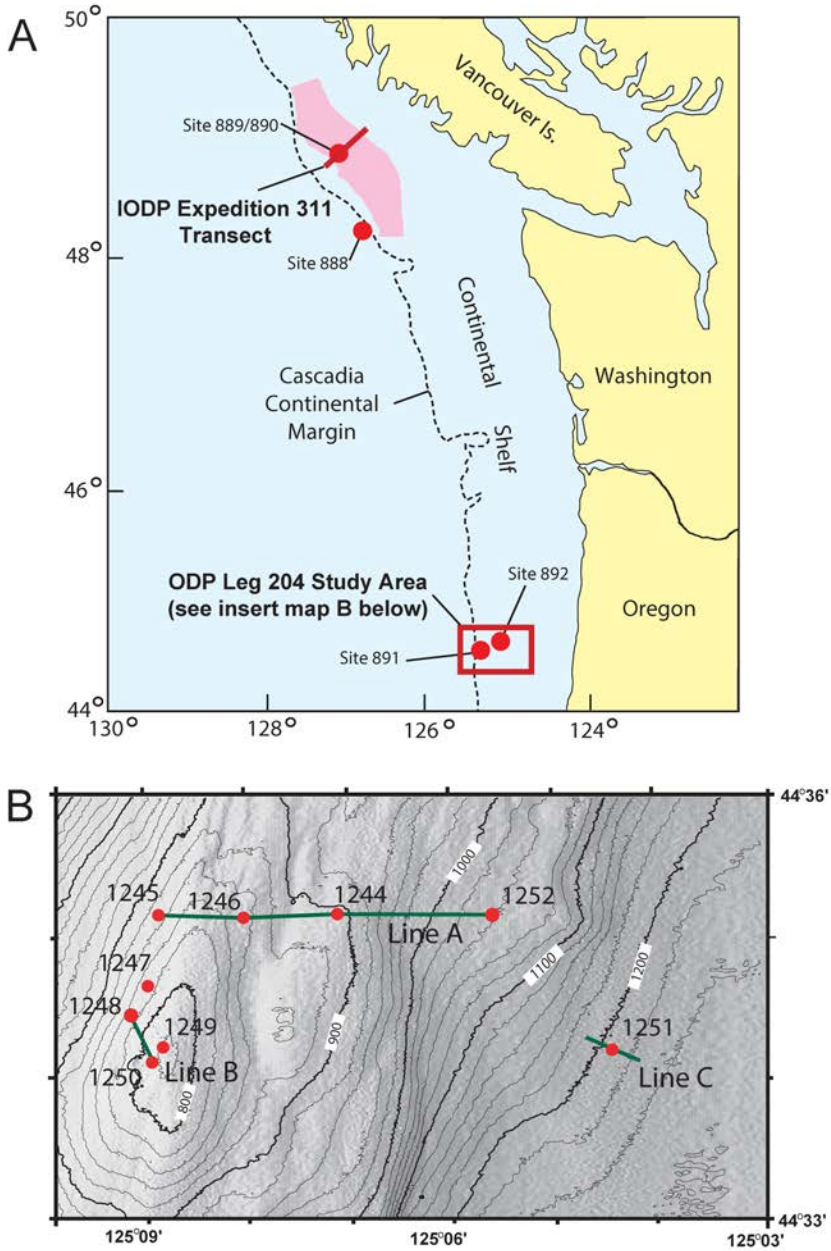

Figure 4.9. (A) Map of the Cascadia continental margin of North America. Locations of ODP Leg 146 drill sites are indicated (Sites 888-892). The location of the IODP Expedition 311 transect and the ODP Leg 204 study area is shown. Also shown is the area (pink shaded area) where methane hydrate occurrence has been mapped on the basis of BSRs (modified from Spence et al., 1995). (B) Insert map of the ODP Leg 204 drill sites along with the location of the seismic profiles depicted in Figure 4.10 (modified from Collett, 2002; Tréhu et al., 2006).

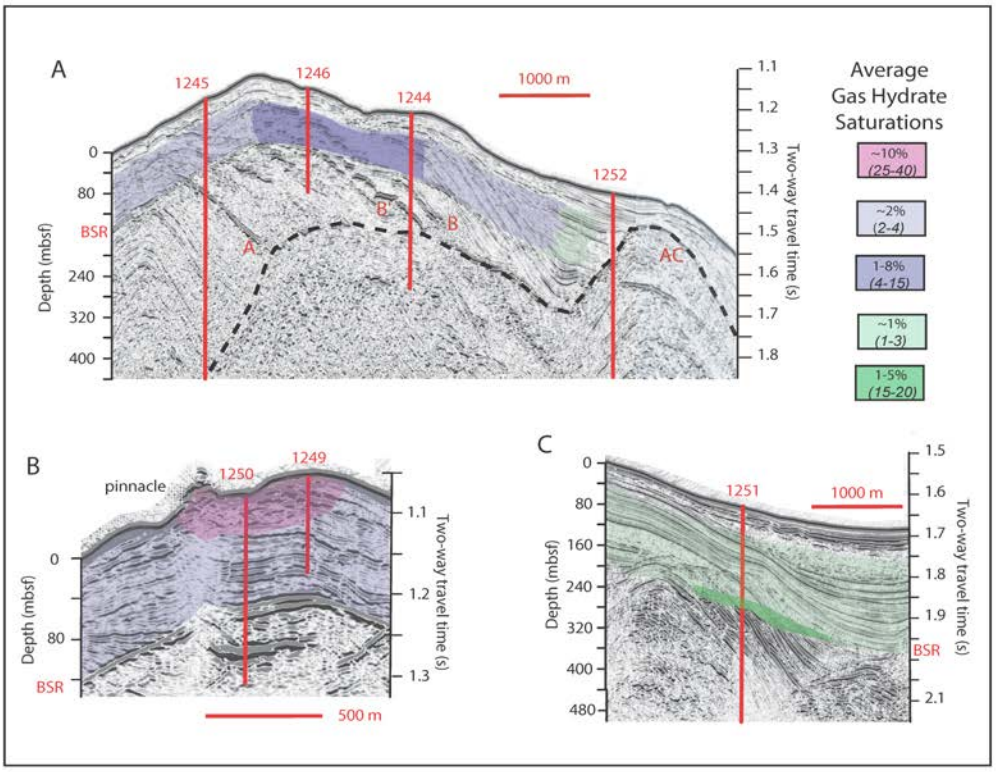

Figure 4.10. Seismic profiles extracted from the 3D seismic data along the lines shown in Figure 4.9. Transparent overlays indicate zones of different average methane hydrate saturations. Vertical red bars show sites drilled during ODP Leg 204. AC = top of the highly deformed sediments of the accretionary complex; B = seismic horizon B, which was found to be coarse-grained and methane hydrate-rich at Site 1246; A = seismic horizon A, interpreted as a stratigraphically controlled zone along which methane (in a free-gas phase) migrates from the accretionary complex to the summit of Hydrate Ridge (modified from Tréhu et al., 2006).

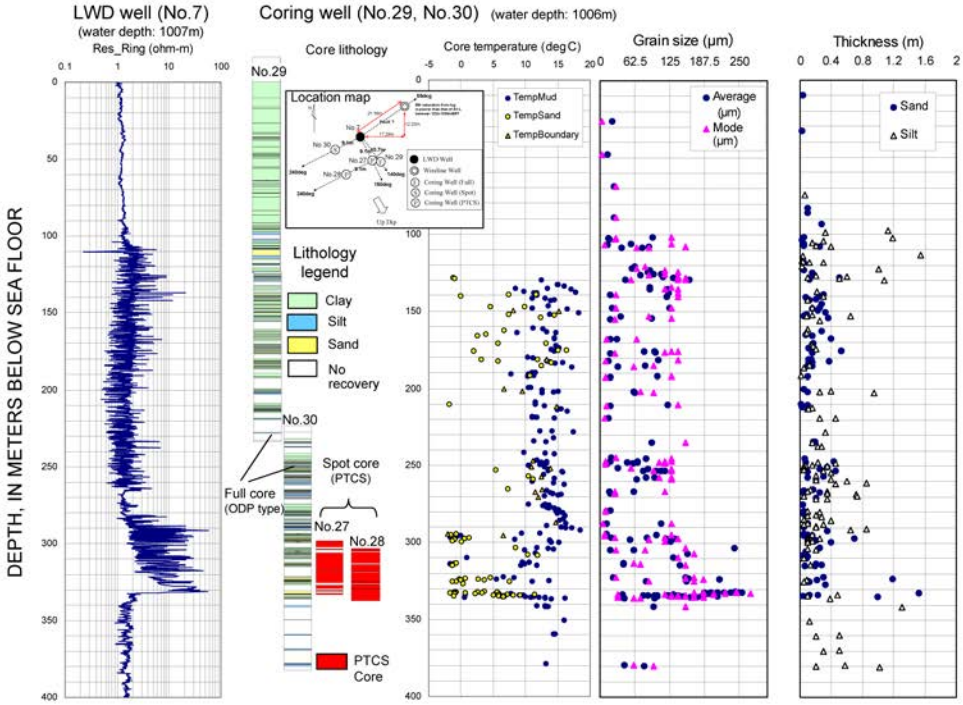

Figure 4.11. Downhole well log and core data display from Site 4, established during the 2004 Tokai-oki to Kumano-nada drilling program (modified from Fujii et al., 2009).

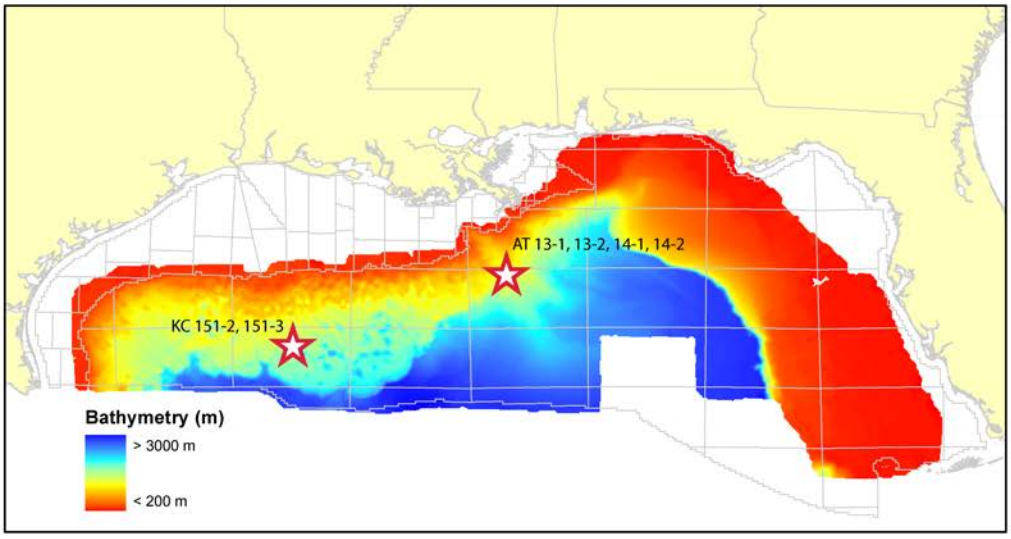

Figure 4.12. Seafloor map of the Gulf of Mexico depicting the location of JIP Leg 1 drill sites (KC151#2, KC151#3, AT13#1, AT13#2, AT14#1, AT14#2).

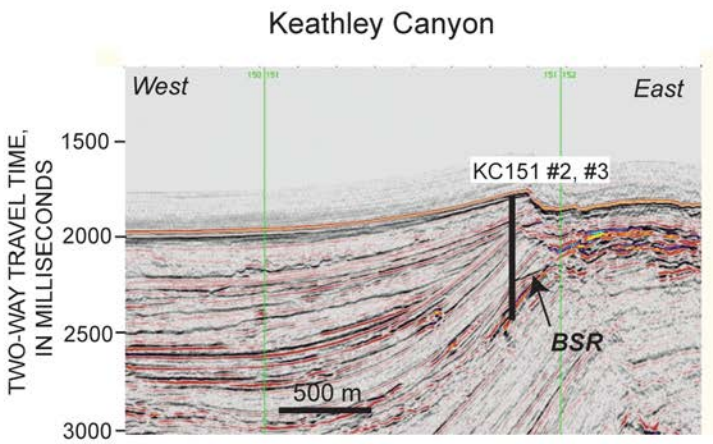

Figure 4.13. Seismic profile depicting the location of the core and logging-while-drilling holes (KC151#2, KC151#3) drilled in Keathley Canyon during the Gulf of Mexico JIP Leg 1. Also shown is the position of a well-developed bottom-simulating reflectors (BSR).

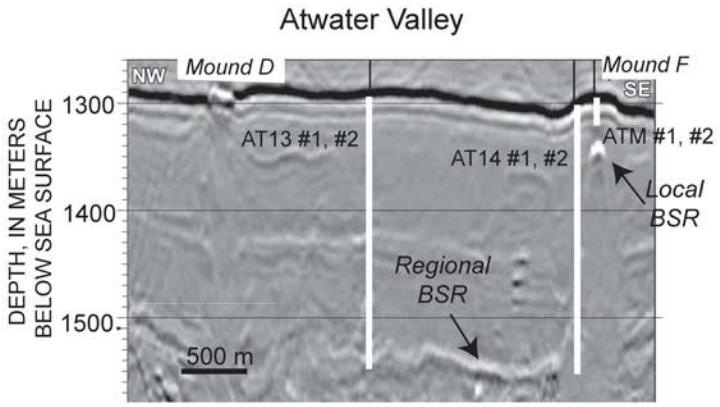

Figure 4.14. Seismic profile depicting the location of the core and logging-while-drilling holes (AT13#1, AT13#2, AT14#1, AT14#2) in the Atwater Valley area during the Gulf of Mexico JIP Leg 1. Also shown is the location of the mound site (Mound F) shallow core holes. BSR = bottom-simulating reflectors

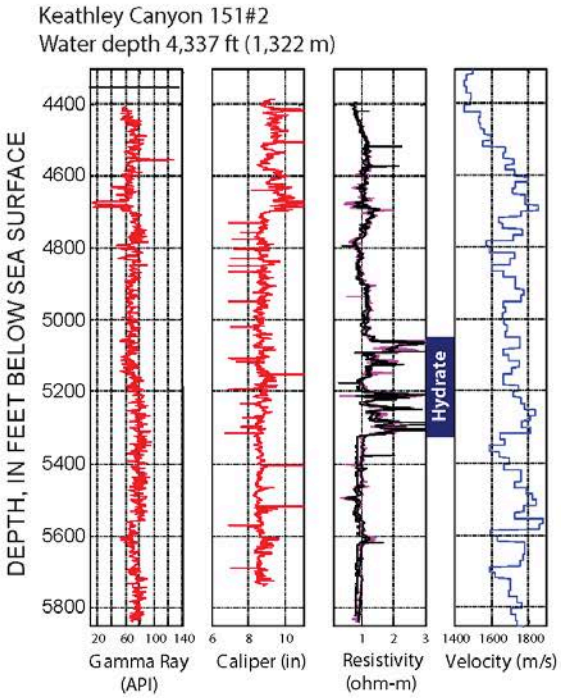

Figure 4.15. Downhole log data from the Keathley Canyon (KC) 151#2 well; depths are from drillers log measured from sea surface. Well log-inferred fracture-filling methane hydrate is in the interval 5,059-5,322 ft from sea surface (sub-seafloor depth of ~220-300 mbsf).

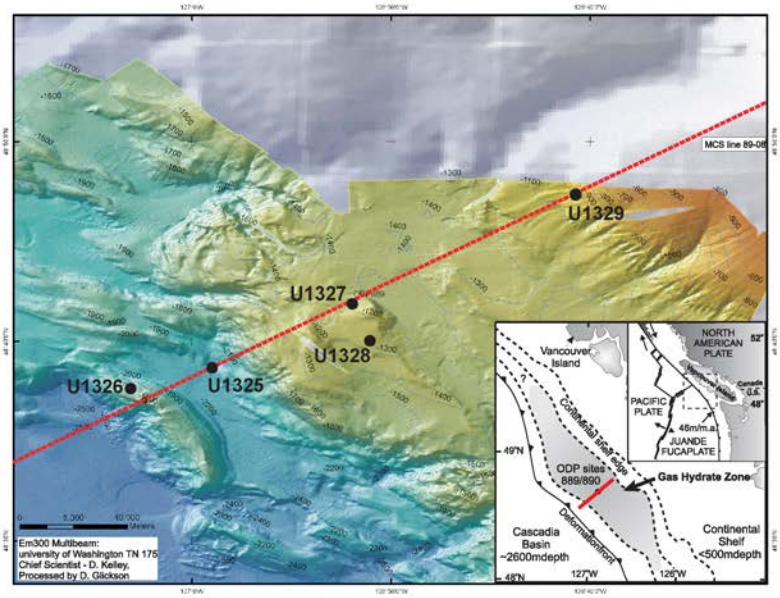

Figure 4.16. Detailed multibeam bathymetry map along the IODP Expedition 311 transect across the accretionary prism offshore Vancouver Island (courtesy of D. Kelly and J. Delaney, University of Washington, and C. Barnes and C. Katnick, NEPTUNE Canada, University of Victoria). Inset shows general location of the drilling transect near previous ODP Sites 889 and 890. A bottom-simulating reflector is present on approximately 50% of the mid-continental slope (shaded area) as inferred from regional multichannel seismic data lines shown in Figure 4.17 and additional regional vintage single channel seismic data (Riedel et al., 2009).

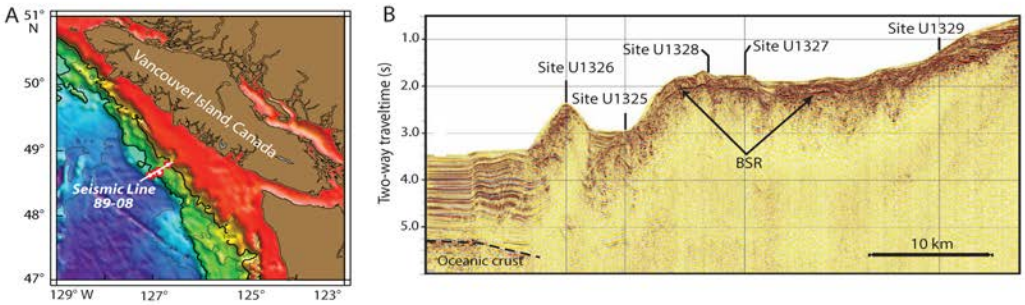

Figure 4.17. (A) Map of the Cascadia continental margin offshore western Canada, showing location of Seismic Line 89-08. (B) Seismic Line 89-08 transect across the northern Cascadia continental margin showing four sites drilled during IODP Expedition 311. The cold vent Site U1328 is ~3 km southeast of the transect line (modified from Torres et al., 2008).

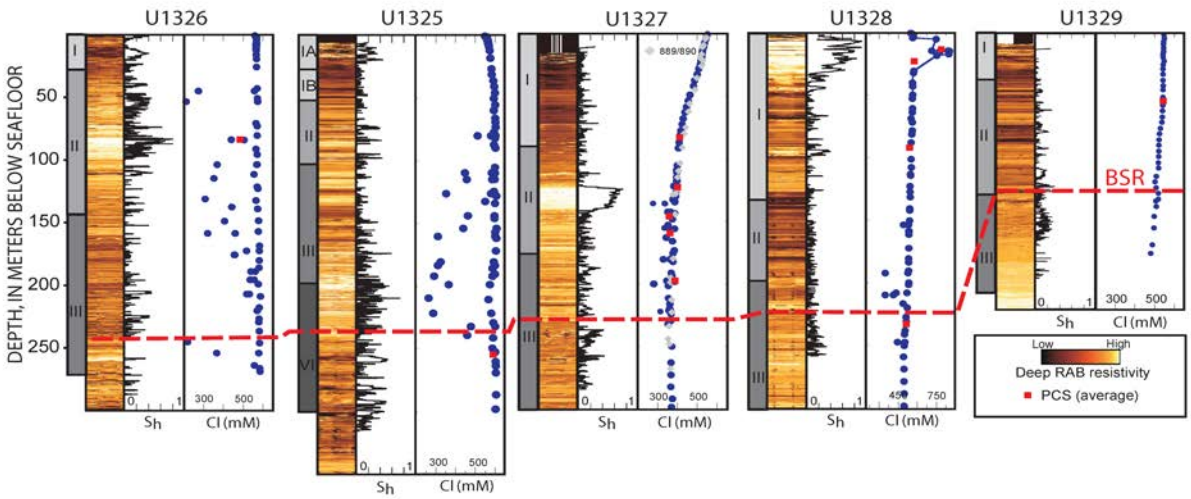

Figure 4.18. IODP Expedition 311 pore water chlorinity profiles (Cl^-) and logging-while-drilling obtained borehole resistivity images. Methane hydrate saturations (S_h) derived from downhole measured resistivity logs. Also shown are lithostratigraphic units and locations of the bottom-simulating reflector (BSR) (Riedel et al., 2009).

Figure 4.19. Gumusut-Kakap field area offshore Sabah, Malaysia (modified from Hadley et al., 2008).

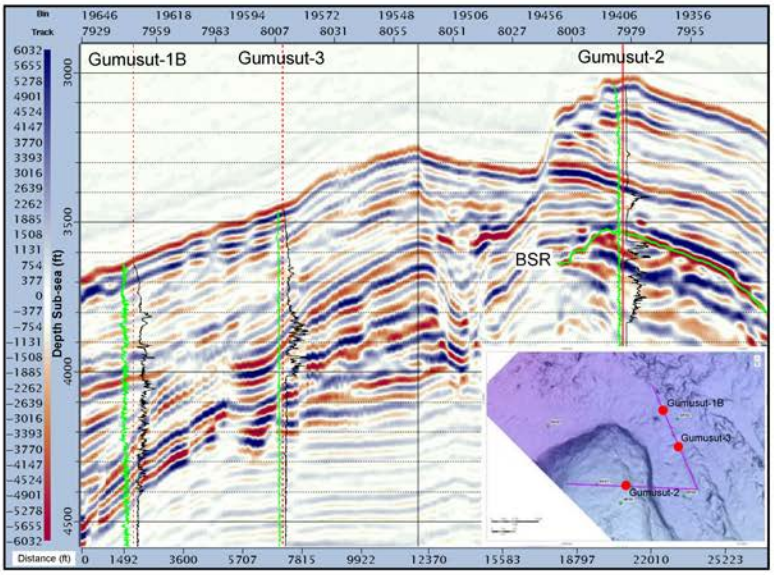

Figure 4.20. Seismic and LWD data across three well locations in the Gumusut-Kakap field area offshore Sabah, Malaysia (modified from Hadley et al., 2008).

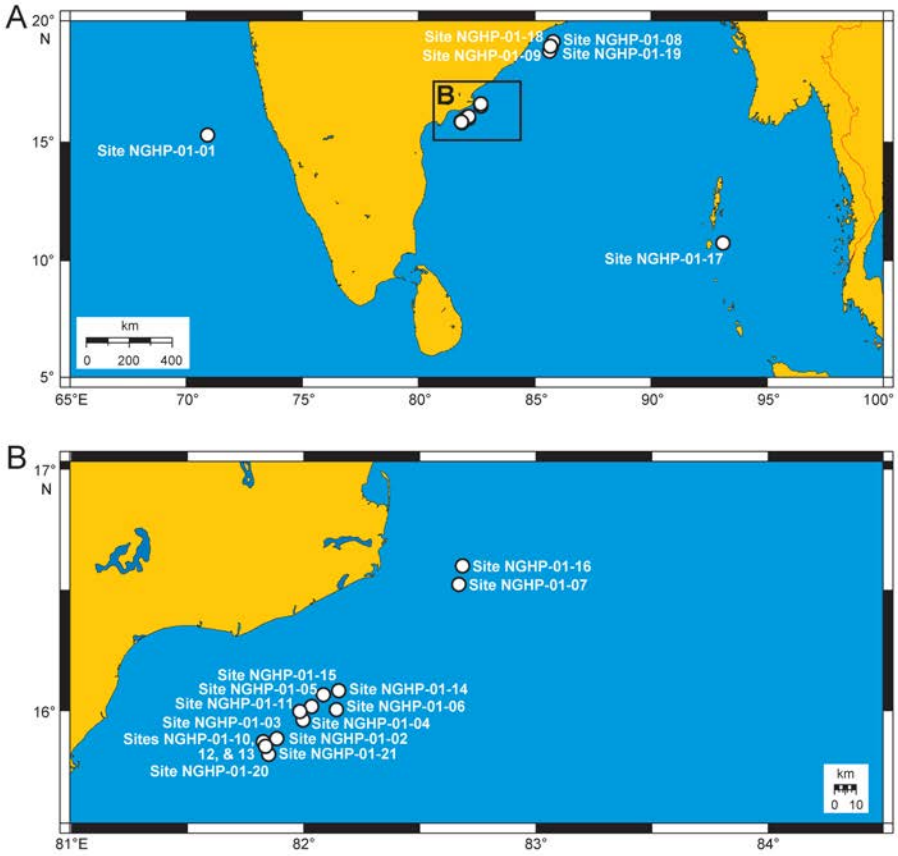

Figure 4.21. (A) NGHP Expedition 01 site map depicting the location of the 21 research drill sites established during the expedition. (B) Insert map of the NGHP Expedition 01 drill sites in the Krishna-Godavari Basin (Collett et al., 2008c).

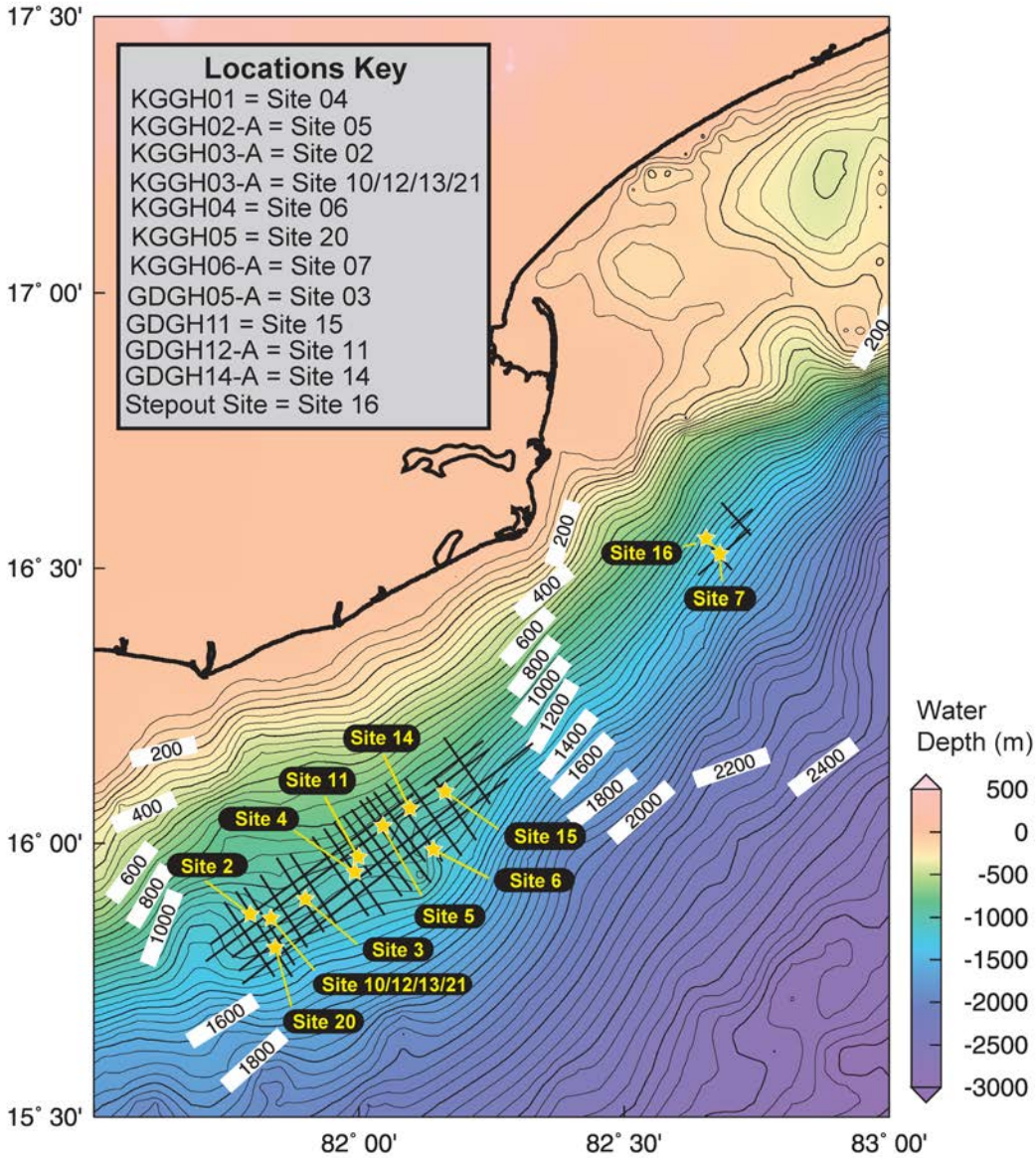

Figure 4.22. NGHP Expedition 01 site map depicting the location of the research drill sites established in the Krishna-Godavari Basin (Collett et al., 2008c).

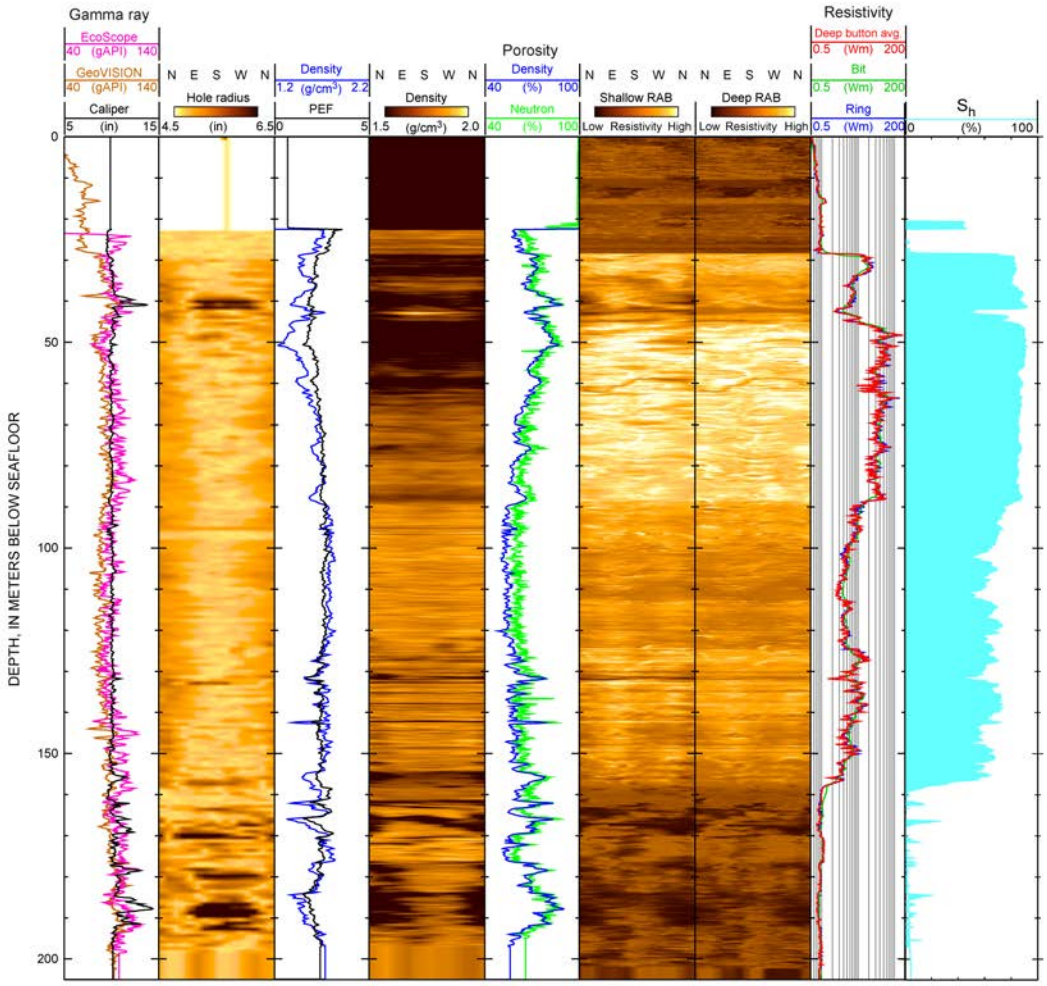

Figure 4.23. Downhole logging-while-drilling data from Hole NGHP-01-10A drilled in the Krishna-Godavari Basin in offshore India (Collett et al., 2008c). Included are the Archie-derived methane hydrate saturations (S_h) as derived from the downhole-measured resistivity log data.

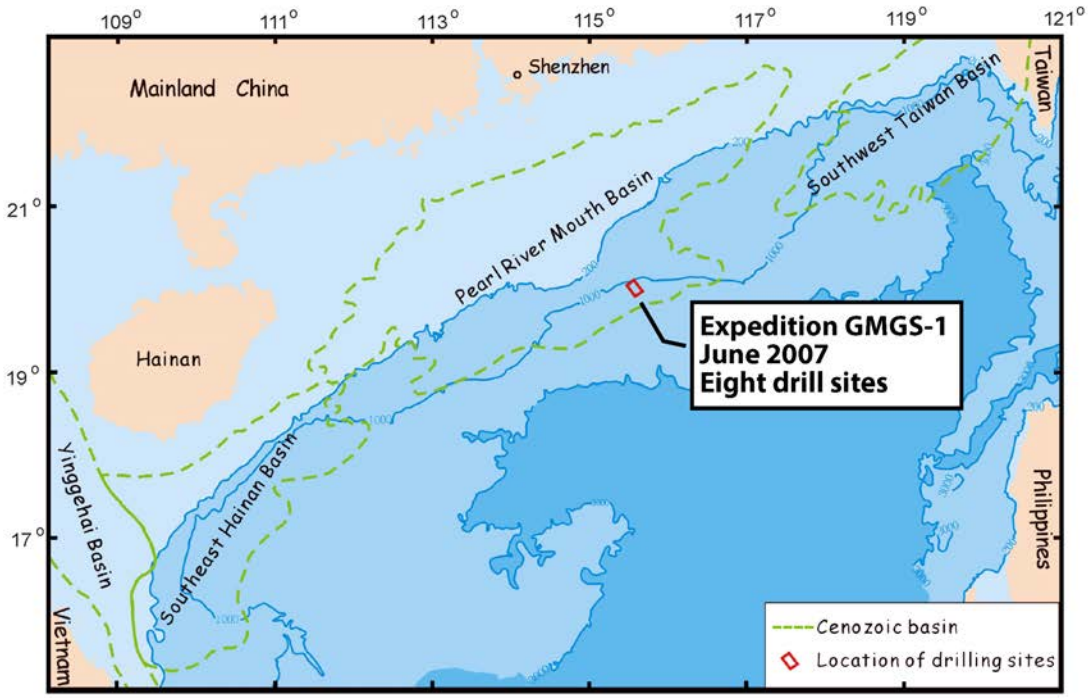

Figure 4.24. Map of drill sites established during Expedition GMGS-1 in the offshore of China in the Shenhu area on the north slope of the South China Sea (modified from Zhang et al., 2007b).

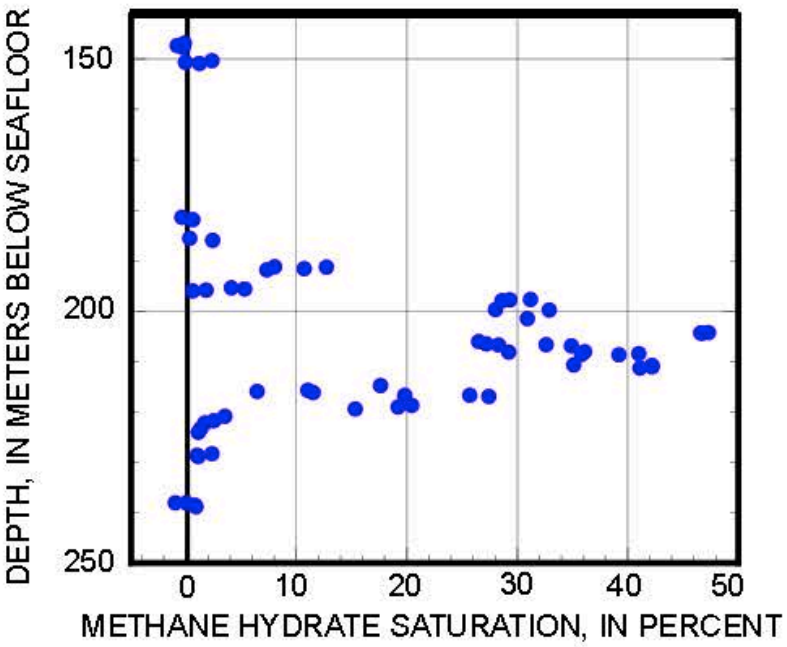

Figure 4.25. Methane hydrate saturations as derived from both pressure core and pore-water freshening analysis from cores obtained during the GMGS-1 expedition in the offshore of China (modified from Zhang et al., 2007b).

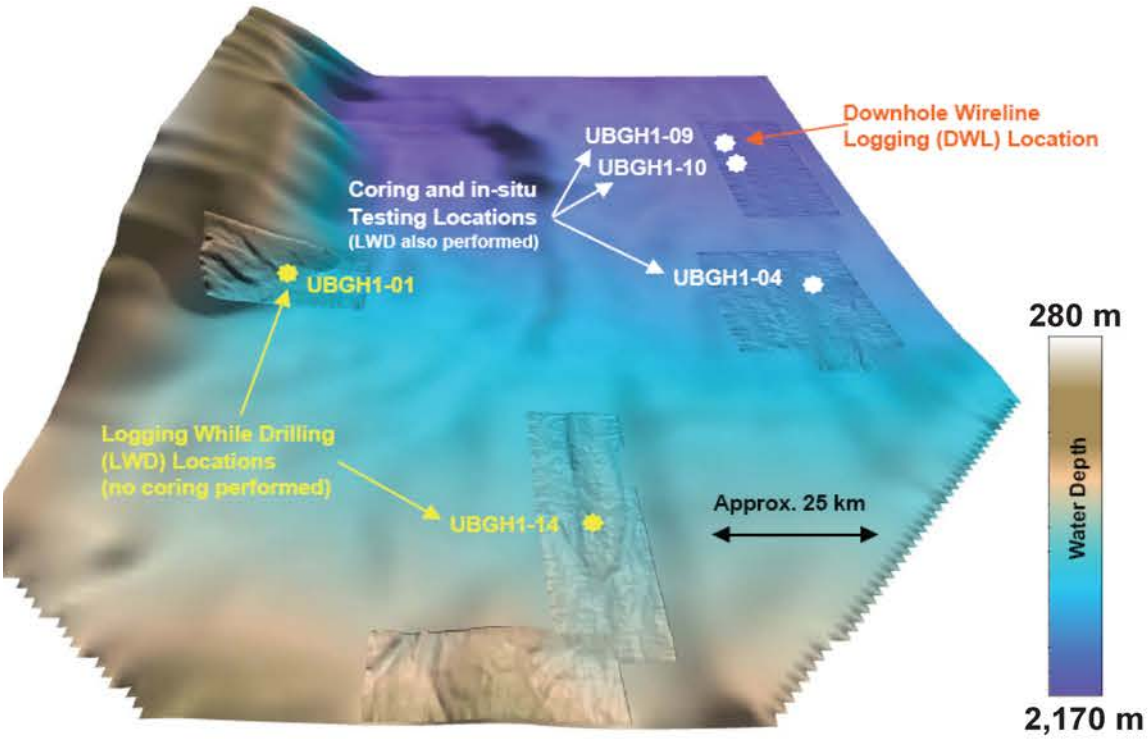

Figure 4.26. Three-dimensional view of the seafloor and drill sites established during Legs 1 and 2 of UBGH1 of the Ulleung Basin Gas Hydrate Expedition 1 (UBGH1) in the Ulleung Basin off the southeast coast of the Republic of Korea (modified from Park et al., 2008).

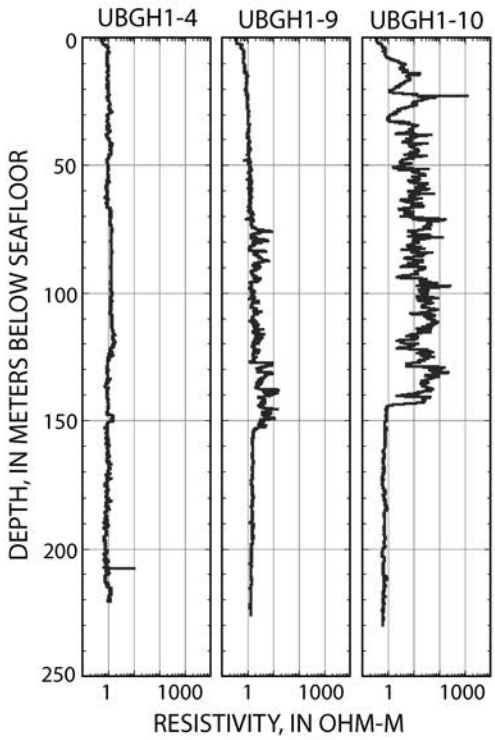

Figure 4.27. Downhole-measured logging-while-drilling resistivity log data (acquired during UBGH1 Leg 1) from the three drill sites cored during UBGH1 Leg 2 (modified from Park et al., 2008). The intervals exhibiting relatively high resistivities (greater than 1 ohm-m) are interpreted to be methane hydrate-bearing.

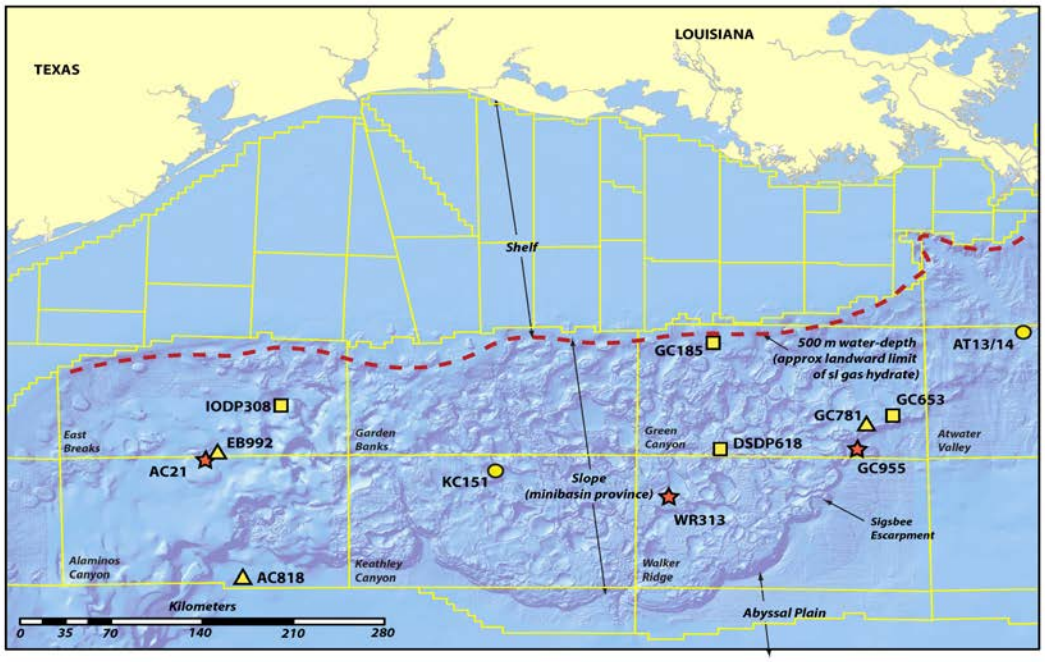

Figure 4.28. Selected methane-hydrate-related sites in the deepwater Gulf of Mexico. Circles denote Gulf of Mexico JIP Leg I (2005) drilling/coring sites. Stars mark Leg II (2009) LWD sites. Additional sites evaluated but not drilled by the JIP are marked by triangles. Squares mark sites associated with other methane hydrate research projects (modified from Boswell et al., 2012a).